Oscillatory and chaotic wakes behind moving boundaries in reaction–diffusion systems

Jonathan A. Sherratt
Nonlinear Systems Laboratory, Mathematics Institute, University of Warwick, Coventry CV4 7AL, UK

(Received February 1996; final version June 1996)

Abstract. *Oscillatory wakes occur in a wide range of reaction–diffusion systems, consisting of either periodic travelling waves or irregular spatiotemporal oscillations, behind a moving transition front. In this paper, the use of a finite boundary moving with an imposed speed to mimic the transition front is considered. For both λ–ω systems and standard predator–prey models, the solutions behind these moving boundaries agree very closely with the behaviour behind transition fronts, provided suitable end conditions are used on the moving boundary. This confirms that the transition front can be regarded as determining the solution, by forcing a particular periodic wave at the boundary of the wake region. In the case of λ–ω systems, a detailed numerical study of solutions on a fixed-length finite domain with a periodic wave solution forced at the boundaries is performed. As the domain length is varied as a parameter, the long-term temporal behaviour undergoes bifurcation sequences that are well known as routes to chaos in ordinary differential equations. This suggests that irregular wakes actually have the form of a perpetual transient in a progression towards chaos. Finally, the way in which the moving boundary results can be used to design an experimental verification of the oscillatory wakes phenomenon in a chemical system is discussed.*

1 Introduction

Oscillatory reaction–diffusion equations have been used to model many biological and chemical systems. Here, 'oscillatory' means that the kinetic ordinary differential equations (ODEs) have a stable limit cycle, reflecting the intrinsic oscillatory behaviour in many real systems, such as the Belousov–Zhabotinskii reaction (Field & Burger, 1985), the intracellular calcium system (Atri *et al.*, 1993;

E-mail: jas@maths.warwick.ac.uk.

0268-1110/96/040303–22

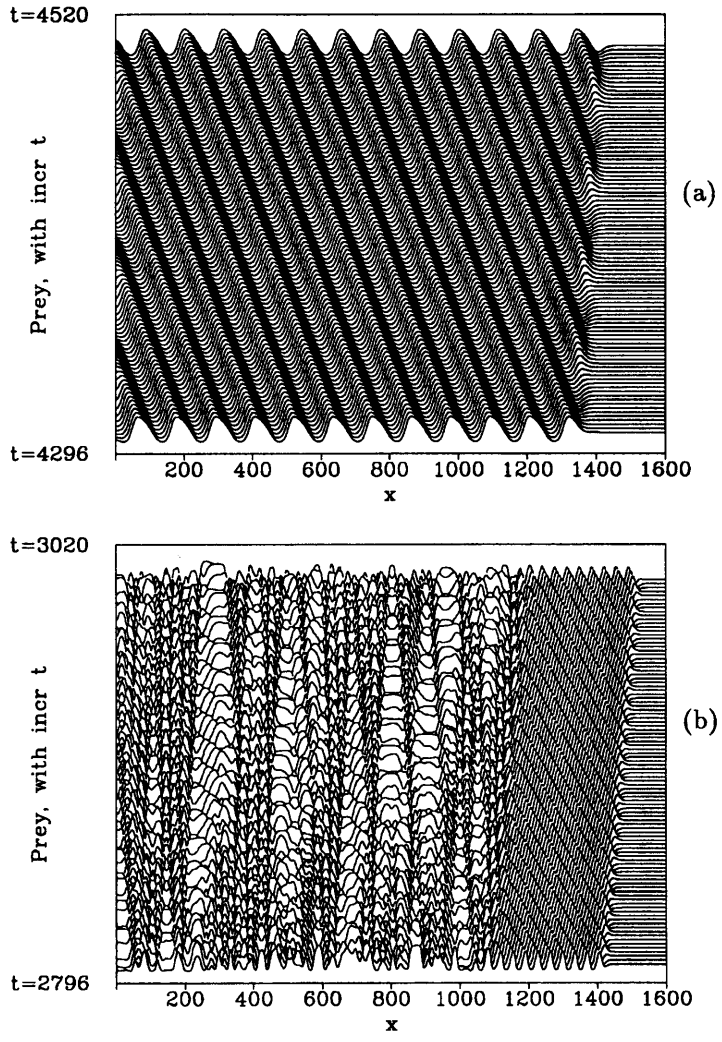

Fig. 1. An illustration of oscillatory wakes. The solutions shown are for a standard predator–prey model $\partial h/\partial t = \partial^2 h/\partial x^2 + h(1-h) - p(1-e^{-Ch})$, $\partial p/\partial t = \partial^2 p/\partial x^2 + Bp(A - 1 - Ae^{-Ch})$, which has oscillatory kinetics for suitable values of the parameters A, B and C (Murray, 1989). The prey density h is plotted as a function of space at successive times, with the vertical separation of successive solutions proportional to the time interval. The solution for predator density p has a qualitatively similar form. Initially, the system is in the coexistence steady state $h = h_s \equiv (1/C)\log[A/(A-1)]$, $p = p_s \equiv Ah_s(1-h_s)$ everywhere except near the $x=0$ boundary, where a small perturbation is introduced. The boundary condition at $x=0$ is zero flux, $p_x = h_x = 0$. This initial perturbation spreads through the domain, leaving behind it an oscillatory wake. In (a), this wake consists of periodic travelling waves; in (b) there are irregular spatio-temporal oscillations, behind a leading band of (unstable) periodic waves. The parameter values are: (a) $A=1.5$, $B=0.05$, $C=4$; (b) $A=1.5$, $B=1$, $C=5$. The equations were solved numerically using the method of lines and Gear's method.

Sanderson *et al.*, 1990) and a number of predator–prey interactions (Breitenmoser *et al.*, 1993; Nisbet & Gurney, 1982). These real systems have a wide range of spatiotemporal behaviours, which have been most widely documented in two spatial dimensions, and include spiral waves, target patterns and spatiotemporal chaos. These are all reflected in two-dimensional solutions of corresponding reaction–diffusion models (Chakravarti *et al.*, 1995; Paullet *et al.*, 1994). However, many questions on the one-dimensional behaviour of oscillatory reaction–diffusion equations remain unanswered, in particular concerning the types of initial data that will evolve to periodic waves and other solution forms, and the possible generation of spatial or temporal chaos. This paper is concerned with a one-dimensional solution form which provides partial answers to both of these questions, and which is here referred to as an oscillatory wake.

Oscillatory wakes arise from very simple initial conditions. Every oscillatory reaction–diffusion system has a homogeneous steady state from which the limit cycle in the kinetics has bifurcated. This steady state is of course unstable, and if a small perturbation is applied, localized in space, this perturbation grows and expands throughout the domain. For simplicity, I consider throughout this paper the case of a semi-infinite domain, with the initial perturbation applied at the finite boundary. The perturbation then induces a transition front moving across the domain, leaving in its wake either regular or irregular spatio-temporal oscillations (Fig. 1). These are the 'oscillatory wakes' that are the subject of this paper. In the case of regular oscillations, the visualizations of the solutions in space–time plots such as in Fig. 1 suggest that these oscillations are in fact periodic travelling waves, and this is confirmed by detailed numerical study (Sherratt, 1994a; Sherratt *et al.*, 1995). The formation of regular or irregular oscillatory wakes in response to localized perturbation occurs in a wide range of oscillatory reaction–diffusion systems, including standard models for intracellular calcium signalling (Sneyd & Sherratt, 1996) and predator–prey interactions (Sherratt *et al.*, 1995). The solution illustrated in Fig. 1 is of a standard reaction–diffusion model for predator–prey dynamics, with different kinetic parameters used in (a) and (b); full details of the equations and parameters are given in the figure legend.

Oscillatory wakes occur behind a leading transition wave front. In this paper, I consider replacing this leading front by a finite boundary moving with an imposed speed, on which a periodic wave solution is forced as a function of time. I begin (Sections 2 and 3) by considering this for 'λ–ω' type reaction–diffusion equations, which are simple prototype oscillatory systems. In previous papers, I have presented a detailed analytical study of oscillatory wakes in λ–ω systems; the purpose of considering the moving boundary simulations for these systems is to determine the extent to which the moving boundary solutions reflect the full semi-infinite-domain behaviour in a case in which this latter behaviour is already well understood. I will show that the similarity between the two solution types is very good, provided care is taken with the end condition on the moving boundary. In Section 4, I continue with λ–ω systems, and discuss the observation of bifurcations to chaos as the length of a finite solution domain is varied as a parameter; these results, in combination with those for moving boundaries, have implications for the nature of the oscillations in irregular wake regions. Finally, in Section 5, I move away from λ–ω systems to describe the application of moving boundary computations to the less well understood case of oscillatory wakes in more general reaction–diffusion systems.

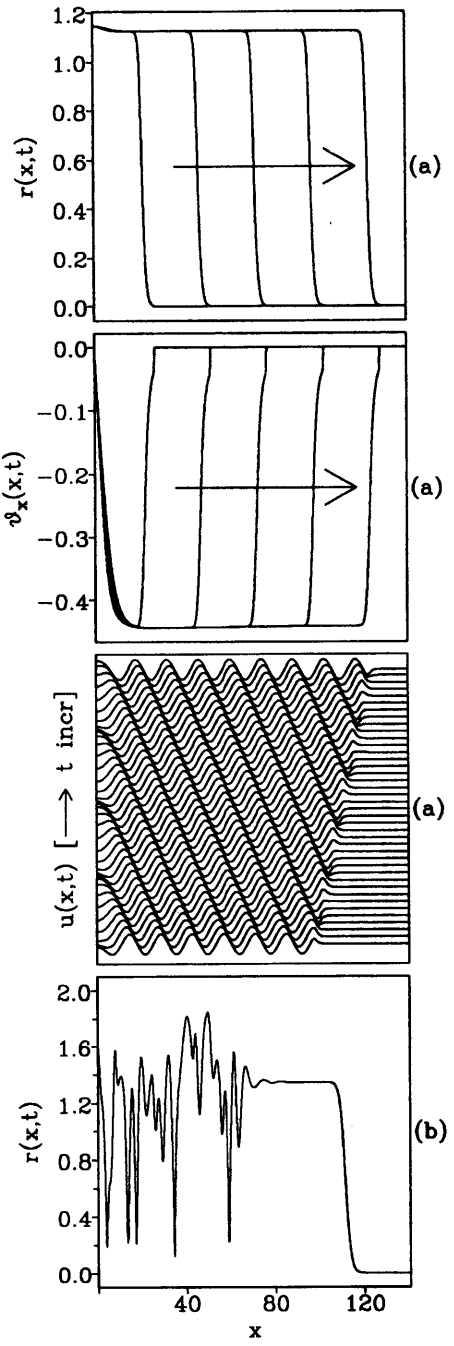

Fig. 2. An illustration of oscillatory wakes in a λ–ω system. The solution plotted is for the system (1) with (a) $\lambda(r)=2-r^5$, $\omega(r)=4-r^2$; (b) $\lambda(r)=2-r$, $\omega(r)=4-r^3$. The solution domain is $0<x<\infty$ with zero flux boundary conditions at $x=0$, and the initial conditions are $u(x,0)=v(x,0)=0.1e^{-\xi x}$ with (a) $\xi=3$, (b) $\xi=1$. In (a) a space–time plot for $u(x,t)$ with $35.6<t<44.5$ is shown, and the solutions for $r(x,t)$ and $\theta_x(x,t)$ as functions of x at equally spaced times is also shown. The solution has the form of simple transition fronts in r and θ_x. In (b) r is plotted as a function of x at $t=38$; in this case, there is a transition to unstable periodic waves, which degenerate into irregular oscillations. The solution for θ_x is qualitatively similar to that for r. The equations were solved numerically using the method of lines and Gear's method.

2 λ–ω Systems on growing domains

The λ–ω class of reaction diffusion systems are equations with the form

$$\frac{\partial u}{\partial t}=\frac{\partial^2 u}{\partial x^2}+\lambda(r)u-\omega(r)v \tag{1a}$$

$$\frac{\partial v}{\partial t}=\frac{\partial^2 v}{\partial x^2}+\omega(r)u+\lambda(r)v \tag{1b}$$

Here u and v are functions of space x and time t, and $r=(u^2+v^2)^{1/2}$. I will consider only the case in which $\lambda(r)$ and $\omega(r)$ are monotonically decreasing, with $\lambda(\cdot)$ having a simple zero at $r=r_0$ and $\omega(0)\neq 0$. These are standard simplifying assumptions for λ–ω systems, and in their absence the oscillatory wake structure can be much more complex (Sherratt, 1993). In fact, there is no additional complication if $\omega(\cdot)$ is monotonically increasing rather than decreasing, but it is convenient to fix on one of these cases. Under these assumptions, the kinetics of (1) have a globally stable circular limit cycle of radius r_0. Moreover, (1) has a one-parameter family of periodic travelling wave solutions, given by

$$u=\tilde{r}\cos\left[\omega(\tilde{r})t\pm\lambda(\tilde{r})^{1/2}x\right] \tag{2a}$$

$$v=\tilde{r}\sin\left[\omega(\tilde{r})t\pm\lambda(\tilde{r})^{1/2}x\right] \tag{2b}$$

with $0<\tilde{r}<r_0$. Any oscillatory reaction–diffusion system has a one-parameter family of periodic travelling waves (Kopell & Howard, 1973), but the ability to write this solution family down in a simple closed form makes λ–ω systems particularly easy to work with, and for this reason they have been used by many authors as prototype oscillatory systems (e.g. Ermentrout, 1980; Koga, 1982). Each of the periodic waves (2) traces out a circular path in the u–v plane, and in fact additional simplification is given by working in polar coordinates r and $\theta=\tan^{-1}(v/u)$ in the u–v plane. In terms of these coordinates, the equations (1) become

$$r_t=r\lambda(r)+r_{xx}-r\theta_x^2 \tag{3a}$$

$$\theta_t=\omega(r)+\theta_{xx}+2r_x\theta_x/r \tag{3b}$$

and the periodic travelling waves are

$$r=\tilde{r},\qquad \theta=\omega(\tilde{r})t\pm\lambda(\tilde{r})^{1/2}x \tag{4}$$

In (3), the subscripts x and t denote partial derivatives.

Systems of the form (1) exhibit both regular and irregular oscillatory wakes, as illustrated in Fig. 2, and the simplicity of the equations enables the wakes to be studied analytically. I will summarize here the results of this work, which is described fully elsewhere (Sherratt, 1994b). In a case such as that illustrated in Fig. 2(a), in which oscillations in the wake are regular, the solution has a very simple form, namely transition wave fronts in r and θ_x (illustrated in Fig. 2). These fronts can be written as $r(x,t)=\hat{r}(x-ct)$, $\theta_x(x,t)=\hat{\psi}(x-ct)$, where c is the front speed. Substituting these solution forms into (3) gives

$$\hat{r}''+c\hat{r}'+\hat{r}\lambda(\hat{r})-\hat{r}\hat{\psi}^2=0 \tag{5a}$$

$$\hat{\psi}'+c\hat{\psi}+2\hat{r}'\hat{\psi}/\hat{r}+\omega(\hat{r})=\kappa \tag{5b}$$

where κ is an arbitrary constant of integration. Ahead of the fronts, $r=\theta_x=0$ ($\Rightarrow u=v=0$), so that $\kappa=\omega(0)$, and behind them, r and θ_x have non-zero values, which are the (unique) non-trivial homogeneous equilibria of (5), given by

$$\theta_x=[\omega(0)-\omega(r)]/c \tag{6a}$$

$$c^2\lambda(r)=[\omega(r)-\omega(0)]^2 \tag{6b}$$

Recall that c is the speed at which the leading transition front moves across the domain. I am considering initial conditions consisting of a small, finite perturbation to the zero steady state near the $x=0$ boundary, and for such initial conditions, simple linearization of (3) about $r=\theta_x=0$ suggests that

$$c=2\lambda(0)^{1/2} \tag{6c}$$

I have confirmed this in a detailed numerical study (Sherratt, 1994b). My monotonicity assumptions ensure that (6b) has exactly one solution on $(0, r_0)$, which I denote by $r=r^*$. In some cases, the periodic waves given by (6) are in fact unstable as solutions of reaction–diffusion equations; an analytical stability condition was derived by Kopell and Howard (1973). It is in precisely these cases that numerical simulations show irregular oscillations. Thus, in these cases, there is a transition front behind which there are periodic waves whose amplitude is given by (6b); however, these waves are unstable and thus further back from the front they degenerate into irregular spatio-temporal oscillations. An example of this is illustrated in Fig. 2(b).

Intuitively, one might expect that when (6) predicts an unstable periodic wave, there would be a second transition, behind the leading front, to a stable periodic wave. One can see in an intuitive way why this does not happen by considering the possibility of such a transition, in the form of a travelling front in solution amplitude. Such fronts have been considered previously by Howard and Kopell (1977). Ahead of this conjectured front, $r\to r^*$ and $\theta_x\to\psi^*\equiv[\omega(0)-\omega(r^*)]/c$, and behind the front $r\to r^{**}$, $\theta_x\to\psi^{**}\equiv\pm\sqrt{\lambda(r^{**})}$, corresponding to a different (stable) periodic wave solution. Assuming that the conjectured front moves with some constant speed a, it will be a function of $x-at$, which can be studied using the ODEs given by replacing c by a in (5).

Using these ODEs, the conditions ahead of and behind the conjectured transition front imply that $a\psi^*+\omega(r^*)=a\psi^{**}+\omega(r^{**})$, so that $a=[\omega(r^{**})-\omega(r^*)]/[\psi^*-\psi^{**}]$. Since $\lambda(\cdot)$ and $\omega(\cdot)$ are monotonically decreasing, r^{**} must be greater than r^* in order that the new periodic wave (of amplitude r^{**}) is stable, so that $\omega(r^{**})<\omega(r^*)$; also $\psi^*>|\psi^{**}|>0$. Together, these imply that a is necessarily negative. Thus, the conjectured second transition front would actually move into the region of stable waves, preserving the unstable region, so that such a front will never occur. A similar argument applies when $\omega(\cdot)$ is monotonically increasing. Note that there is an explicit spatial polarity in this calculation—the direction of movement of the conjectured front would be the same if the lower amplitude waves were behind the front. This spatial polarity is provided simply by the direction of motion of the periodic waves.

In this discussion of the formation and stability of oscillatory wakes in λ–ω systems, I have referred to the wake region almost as a separate entity. However, this is clearly not the case: the wake is a part of the whole reaction–diffusion

solution, and to treat it separately is just an intuitive device. Searching for a way to explore the validity of this device, I consider solving the reaction–diffusion system on a finite but growing domain, $0<x<c_{\text{bndy}}t$, where c_{bndy} is a positive constant. This finite domain is intended to represent the wake region in isolation, and thus I take the boundary condition on the stationary boundary $x=0$ to be the same as in the semi-infinite-domain solutions, namely $u_x=v_x=0$; however, the boundary condition on the moving boundary requires careful consideration.

The basic hypothesis that I have made in the preceding discussion of oscillatory wakes is that the behaviour in the wake region is forced by the rear of the advancing transition front. Thus, it is natural to consider boundary conditions on the moving boundary which force a particular periodic plane wave. Since a periodic wave is determined uniquely by the (constant) value of θ_x, it is natural to use boundary conditions

$$r_x=0 \quad \text{and} \quad \theta_x=\lambda(r^*)^{1/2} \quad \text{at} \quad x=c_{\text{bndy}}t \tag{7}$$

which converts to a simple condition on u_x and v_x. This boundary conditions forces periodic waves of amplitude r^* moving in the negative x direction. There are, of course, other boundary conditions which would force periodic waves and I will consider some of these alternatives in Section 3.

Figure 3 illustrates the numerical solution of this moving-boundary problem for three different sets of functions $\lambda(\cdot)$ and $\omega(\cdot)$; the numerical methods used are discussed in the appendix. Here the amplitude r^* at the moving boundary is calculated using (6), with c_{bndy} taken as the wave front speed $c=2\lambda(0)^{1/2}$, and in Fig. 3, the moving-boundary solutions are compared with the solutions of the corresponding semi-infinite-domain problem. The comparison between the solutions is extremely good. In Fig. 3(a), the periodic waves of amplitude r^* are stable and, as one would expect intuitively, the moving-boundary solution consists of these periodic waves, as does the wake region of the semi-infinite-domain solution. For the $\lambda(\cdot)$ and $\omega(\cdot)$ used in Fig. 3(b), waves of amplitude r^* are unstable, and in this case both solutions consist of a band of periodic waves, with irregular oscillations further back. Remarkably, the width of the band of regular oscillations in the moving-boundary solution is the same as in the oscillatory wake region of the semi-infinite-domain solutions.

An equally good comparison is shown for a wide range of forms for $\lambda(\cdot)$ and $\omega(\cdot)$; however, the analytical description of the semi-infinite-domain solutions for λ–ω systems in terms of travelling fronts in r and θ_x means that this good comparison is entirely expected. More surprising are the results illustrated in Fig. 3(c), in which irregular oscillations occur immediately behind the leading transition front in the semi-infinite-domain solution, without any intermediate band of regular oscillations. This also occurs in the moving-boundary solutions, even though periodic waves of amplitude given by (6) are forced on the boundary; the explanation is that these periodic waves are highly unstable. The quality of the comparisons in all three parts of Fig. 3 provides strong evidence that the oscillatory wakes in solutions such as those illustrated in Fig. 2 are indeed induced by a forcing of a periodic wave at the rear of the leading transition front, even when the wake region is entirely irregular.

The details of the irregular oscillations are, of course, different in the two solutions shown in Fig. 3(b), and also in Fig. 3(c). This is entirely expected. I will present evidence (in Section 4) suggesting that these irregular oscillations in fact become genuinely chaotic as $t\to\infty$, which implies that a numerical solution will

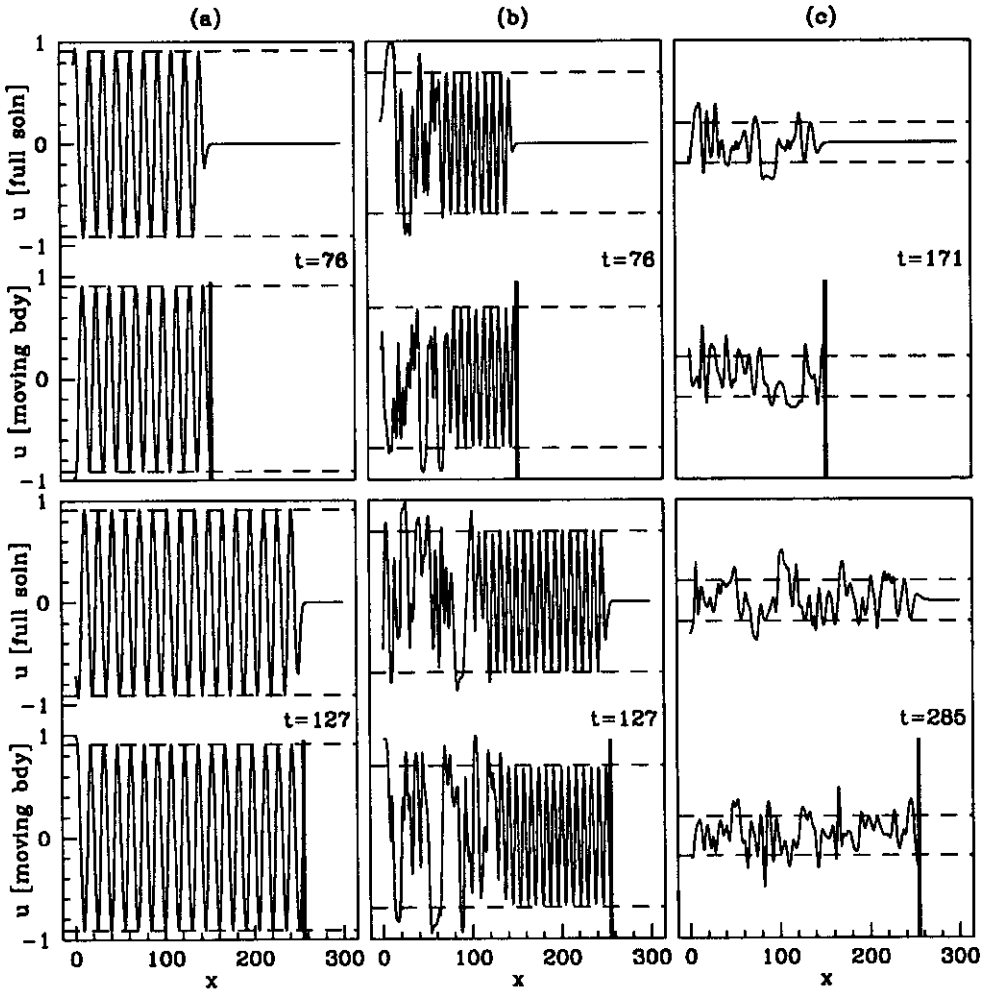

Fig. 3. A comparison between semi-infinite-domain (marked 'full soln') and moving-boundary solutions for λ–ω systems (1) with $\lambda(r)=a(1-r^2)$, $\omega(r)=3-br^2$ and (a) $a=b=1$; (b) $a=1$, $b=3$; (c) $a=0.2$, $b=10$. The boundary condition on the moving boundary is (7) with $c_{bndy}=2$, which is the speed $2\lambda(0)^{1/2}$ at which the transition front moves in the semi-infinite-domain solution (Sherratt, 1994b). The value of r^* is taken from (6) and is indicated by dashed lines; the location of the moving boundary is shown by a solid line. The solutions are plotted as a function of x at two times t. The equations were solved numerically using a Crank–Nicolson finite difference scheme, as discussed in the appendix.

never be a good approximation to an exact solution, whatever the accuracy of the numerical method. Thus, in these cases, numerical solutions give only qualitative information about the form of the true solution.

In the semi-infinite-domain solutions, the speed of the leading front and the amplitude of the periodic waves behind it are linked by the equation (6b). However, in the moving-boundary case there is no such relationship, and the speed c_{bndy} of the moving boundary can be varied independently of the wave amplitude r^*. When the waves of amplitude r^* are stable, this variation has no significant effect on the solution, but in an unstable case, the effect is marked, as illustrated in Fig. 4. As the boundary speed decreases, the width of the band of periodic waves

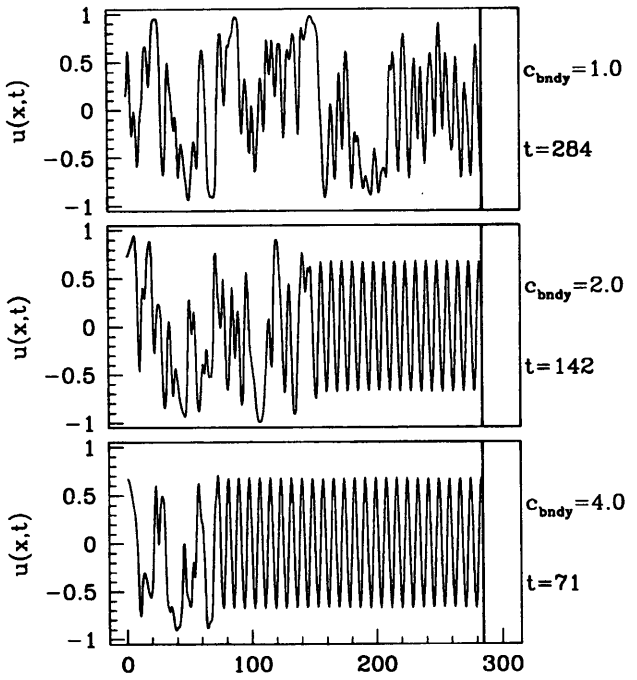

Fig. 4. The effect of the boundary speed c_{bndy} on the moving-boundary solution. The solutions shown are for (1) with $\lambda(r) = 1 - r^2$ and $\omega(r) = 3 - 3r^2$. The boundary condition on the moving boundary is (7), with r^* calculated using (6) (this is independent of c_{bndy}). As the boundary speed decreases, the width of the band of periodic waves immediately behind the moving boundary also decreases. The equations were solved numerically using a Crank–Nicolson finite difference scheme, as discussed in the appendix.

also decreases, and disappears altogether at low speeds. Similar results are obtained for a range of forms for $\lambda(\cdot)$ and $\omega(\cdot)$. In the same way, a wave amplitude other than r^* can be used in the moving-boundary condition (7); the wake region consists of periodic waves of whatever amplitude is imposed at the boundary, with irregular oscillations further back if these waves are unstable.

The idea of reformulating wave propagation problems in reaction–diffusion systems as moving-boundary-value problems is not new. Norbury and Stuart (1988, 1989) used this technique to study porous medium combustion, by restricting attention to the region of finite (but time-varying) length in which the reaction occurs. The essential difference between their approach and mine is that Norbury and Stuart's reduction is exact; it is made possible by the details of their equations. In contrast, I am using moving-boundary solutions as an intuitive device to aid understanding of qualitative behaviour.

3 Other conditions on the moving boundary

The relation (7) is a natural candidate for a boundary condition that forces periodic waves. However, there are some other intuitively plausible candidates, and I will discuss two of these in this section. Recalling the form (4) for a periodic wave solution of a λ–ω system, one possible condition on the moving boundary is $r_x = 0$, $\theta_x = \lambda(r)^{1/2}$. This is a generalization of (7), which forces the solution to have the form of a periodic wave, but does not select a particular periodic wave. Numerical

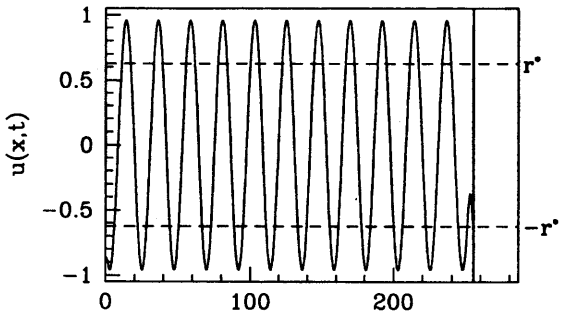

Fig. 5. An example of the moving-boundary solutions with condition (10) on the moving boundary, and $c_{bndy}=2$. The value of r^* is calculated using (6), and is indicated by dashed lines. The solution has the form of periodic waves with amplitude r_{extra}, given by (12), which is significantly greater than r^*. In this simulation, $\lambda(r)=1-r^2$ and $\omega(r)=3-4r^2$. The equations were solved numerically using a Crank–Nicolson finite difference scheme, as discussed in the appendix.

solutions of the moving-boundary problem with this boundary condition at $x=c_{bndy}t$ for a wide range of $\lambda(\cdot)$ and $\omega(\cdot)$ simply give spatially homogeneous oscillations in u and v, so that $r\equiv r_0$ and $\theta_x\equiv\lambda(r_0)=0$. This is simply the limit cycle solution of the kinetics. Therefore, oscillatory wakes cannot be generated simply by a moving-boundary condition that is consistent with periodic waves; a particular wave must be forced on the moving boundary.

With this in mind, I consider a second alternative condition on the moving boundary, in which the values of u and v are imposed as functions of time, specifically

$$u=r^*\cos[\omega(r^*)t+\lambda(r^*)^{1/2}x] \text{ and } v=r^*\sin[\omega(r^*)t+\lambda(r^*)^{1/2}x] \text{ at } x=c_{bndy}t \quad (8)$$

As one might expect, this condition successfully forces periodic waves of amplitude r^*, and gives results that are essentially identical to those obtained with (7) (not illustrated for brevity). Of course, when irregular oscillations occur, there are differences in the detail of these, as expected. Thus, the boundary conditions (7) and (8) both give solutions with the same form as the oscillatory wake in the corresponding semi-infinite-domain solution.

Another natural case to consider is the use of conditions on the moving boundary which force periodic waves moving in the positive x direction, that is either

$$u=r^*\cos[\omega(r^*)t+\lambda(r^*)^{1/2}x] \text{ and } v=r^*\sin[\omega(r^*)t+\lambda(r^*)^{1/2}x] \text{ at } x=c_{bndy}t \quad (9)$$

$$\text{or } r_x=0 \text{ and } \theta_x=-\lambda(r^*)^{1/2} \text{ at } x=c_{bndy}t \quad (10)$$

I must stress immediately that these conditions do not correspond to any semi-infinite-domain computations. Numerical simulations with conditions (9) or (10) on the moving boundary give the same results, but these results have a rather unexpected form. Periodic waves do form behind the moving boundary, but their amplitude is significantly greater than r^* (Fig. 5). Moreover, the waves move in the negative x direction, opposite to the direction that is forced at the boundary, although this cannot be seen in Fig. 5.

This initially surprising result can be explained by a detailed consideration of (9).

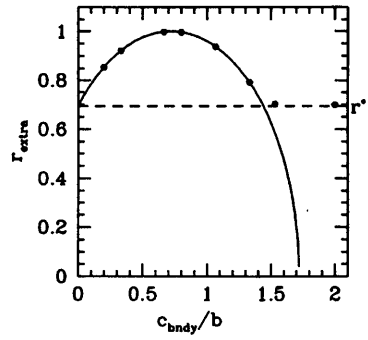

Fig. 6. An illustration of the variation of r_{extra}, defined in (12) with c_{bndy}/b (solid curve). This curve applies to the case $\lambda(r)=1-r^2$, $\omega(r)=3-br^2$. Also shown is (points) the periodic wave amplitude observed in numerical moving-boundary simulations for $b=3$, using boundary condition (10) on the moving boundary. In both (12) and (10), the value of r^* is calculated using (6), and is shown as a dashed line. The numerically observed wave amplitude is the larger of r^* and r_{extra}. The equations were solved numerically using a Crank–Nicolson finite difference scheme, as discussed in the appendix.

This boundary condition imposes $r=r^*$ and also specifies θ as a function of t. Is it possible that more than one periodic wave has the same form for θ as a function of t on the moving boundary? To answer this, we must look for solutions of

$$\omega(r)\pm\lambda(r)^{1/2}c_{bndy}=\omega(r^*)-\lambda(r^*)^{1/2}c_{bndy} \tag{11}$$

Clearly, $r=r^*$ is a solution, but there may be others. The number of solutions in fact depends on $\lambda(\cdot)$ and $\omega(\cdot)$ and to be specific I focus on the case $\lambda(r)=1-r^2$, $\omega(r)=3-br^2$; the solutions in Figs 3(a), 3(b), 4 and 5 are all for functions of this form, with different values of b. In this case, (11) can be solved exactly, giving one solution in addition to $r=r^*$, namely

$$r=r_{extra}\equiv\left[(r^*)^2+\frac{c_{bndy}}{b}\left(2\sqrt{1-(r^*)^2}-\frac{c_{bndy}}{b}\right)\right]^{1/2} \tag{12}$$

This is exactly the larger periodic wave amplitude in the solutions illustrated in Fig. 5, and waves of this amplitude are also induced by boundary condition (10).

As c_{bndy}/b increases from zero with fixed r^*, r_{extra} initially increases from r^*, reaching a maximum value of 1 at $c_{bndy}/b=\lambda(r^*)^{1/2}$. The value of r_{extra} then starts to decrease, reaching the value r^* again at $c_{bndy}/b=2\lambda(r^*)^{1/2}$, and becoming zero at $c_{bndy}/b=1+\lambda(r^*)^{1/2}$. This variation is illustrated for one particular value of r^* in Fig. 6. Also in this figure is plotted the periodic wave amplitude observed in numerical solutions of the moving-boundary problem with boundary condition (9) for $b=3$, as c_{bndy} is varied. For all values of c_{bndy}/b, the observed amplitude is the larger of r^* and r_{extra}. I have experimented numerically with a number of different forms $\lambda(\cdot)$ and $\omega(\cdot)$, and in all cases the same rule applies: the observed solution consists of periodic waves, whose amplitude is given by the largest root of (11) on $(0, r_0]$. I have no formal argument as to why this should be so, although if one conjectures an amplitude transition front between r^* at $x=c_{bndy}t$ and r_{extra} at smaller x, the argument used in Section 2 shows that this front will move in the negative x direction (away from the front) unless $r_{extra}>r^*$; thus, one does not expect waves

of amplitude r_{extra} when $r_{\text{extra}} < r^\star$. I must emphasize that when an amplitude other than $r^\star$ is selected, there is a boundary layer at the moving boundary, since for (9), $r = r^\star$ on the boundary, and for (10), $\theta_x < 0$ on the boundary.

Finally in this section, I should comment that in the light of the preceding discussion, it will come as no surprise that the condition

$$u = \cos[\omega(r^\star)t] \quad \text{and} \quad v = \sin[\omega(r^\star)t] \tag{13}$$

at the moving boundary does not induce periodic waves of amplitude $r^\star$. This prescription of the temporal form of the periodic wave is effective at forcing waves on a stationary boundary, but once the boundary moves, this movement must be taken into account. In fact, numerical simulations suggest that (13) forces periodic waves whose amplitude is given by the largest root of

$$\omega(r) \pm \lambda(r)^{1/2} c_{\text{bndy}} = \omega(r^\star)$$

This equation will always have at least one root in $(0, r_0)$ provided $\lambda(\cdot)$ and $\omega(\cdot)$ are monotonic.

4 Bifurcation studies for λ–ω systems

In Sections 2 and 3, I have presented evidence indicating that oscillatory wakes behind transition fronts in λ–ω systems can be well represented by corresponding solutions on growing domains, provided a suitable boundary condition is used on the moving boundary. I will now use this fact to gain a preliminary insight into the nature of the spatio-temporal irregularities observed in some wake regions. The first step in this process is to consider solutions on a fixed-length, finite domain, say $0 < x < L$; I will return to growing domains in due course. I consider such solutions with the boundary condition (7) applied at both boundaries; since these boundaries are stationary, (7) is in fact equivalent to (10), via the transformation $x \mapsto -x$.

I have previously considered the way in which the long-term behaviour of such solutions varies as $r^\star$ is varied with a fixed domain length L (Sherratt, 1995). However, the moving-boundary results suggests that it may be more appropriate to fix $r^\star$ and consider varying the domain length. I must stress that here the domain length is a parameter which I am varying, and is not a function of time. For any given $r^\star$, the periodic wave solution $r \equiv r^\star$, $\theta_x \equiv \lambda(r^\star)^{1/2}$ will be stable as a solution of (1) on $0 < x < L$ subject to (7) at $x = 0$ and $x = L$, provided L is sufficiently small. I have previously outlined a method enabling calculation of the value of L at which the stability changes (Sherratt, 1995). My interest here is in the long-term behaviour that results when L is increased above this critical value. This is entirely a numerical study, and the fact that I am concerned with long-term behaviour means that it is computationally very expensive. For this reason I have focused almost exclusively on one set of $\lambda(\cdot)$ and $\omega(\cdot)$, namely $\lambda(r) = 1 - r^2$ and $\omega(r) = 3 - r^2$ (chosen arbitrarily), and I will describe the results for this case only. In contrast to the numerical results in Section 2 and 3, I have little evidence concerning the generality of the results presented in this section.

When L is just above the critical value for stability, the form of the long-term solution can actually be calculated from linear analysis of (3), and has the form of periodic temporal oscillations in r and θ_x at all space points. The subsequent change in long-term behaviour as L is increased further is illustrated in Figs 7 and

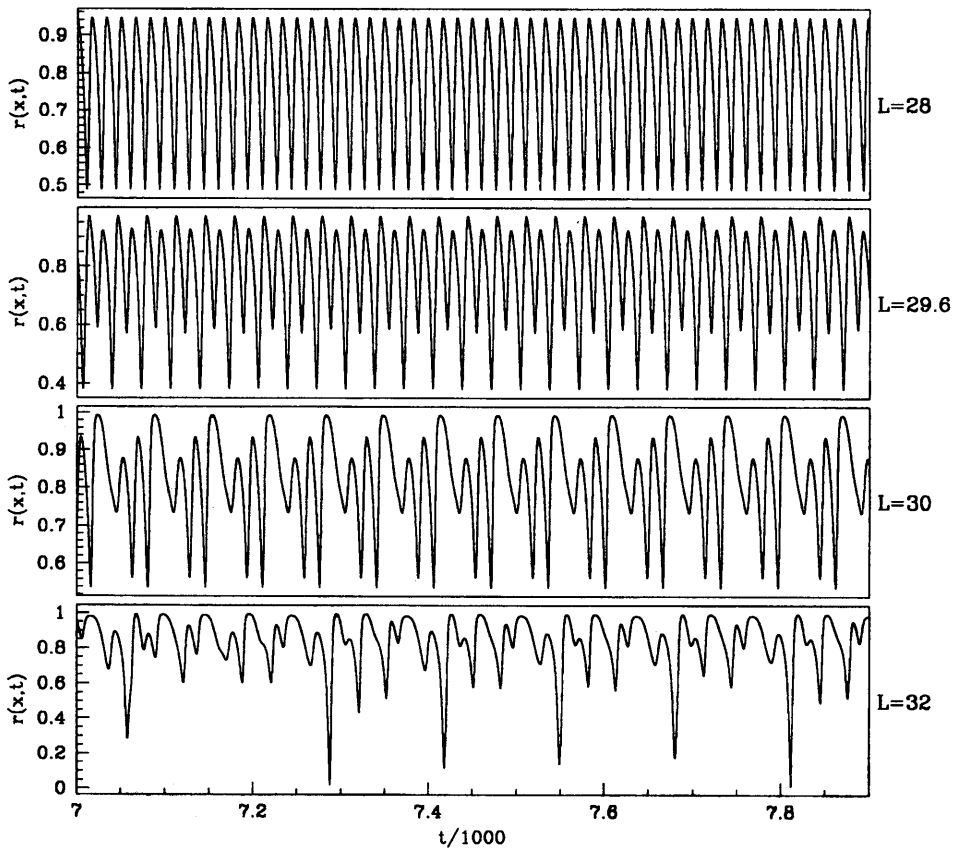

Fig. 7. Bifurcations in the long-term behaviour of λ–ω solutions on a finite domain. The solutions illustrated are for equations (1) with $\lambda(r)=1-r^2$, $\omega(r)=3-r^2$ on $0<x<L$, subject to boundary condition (7) at $x=0$ and $x=L$, with $r^*=0.8075$. The solution for r is plotted as a function of time t at $x=L/11$. The long-term behaviour is essentially independent of initial conditions. As L is increased, the long-term temporal behaviour changes from r constant (corresponding to periodic waves in u and v, not shown) to periodic temporal oscillations in r. The period of the oscillations then doubles several times before the behaviour becomes irregular. The various transitions appear to occur synchronously in space, but the amplitude of r variations decreases with x; thus, for maximum clarity the plotting is at a position close to the $x=0$ boundary. The equations were solved numerically using the method of lines and Gear's method.

8 for $r^*=0.8075$ and 0.535 respectively. In the former case, the simple temporal oscillations in r and θ_x become unstable at $L\approx 29$, via period doubling. This is the onset of a period-doubling cascade (I have observed two further doublings numerically), and for L greater than about 31, the long-term behaviour consists of irregular temporal oscillations. This period-doubling sequence appears to occur synchronously at all space points, and in Fig. 7 I plot the solution for one value of x only.

For $r^*=0.535$, the sequence of bifurcations (Fig. 8) is rather different. Here the periodic wave solution loses stability at $L\approx 5$, again giving temporal oscillations in r and θ_x at all space points. These in turn become unstable at $L\approx 24$, but this is not through period doubling, but rather through what appears to be a bifurcation to a torus. As L is increased, this transition leads gradually to irregular temporal

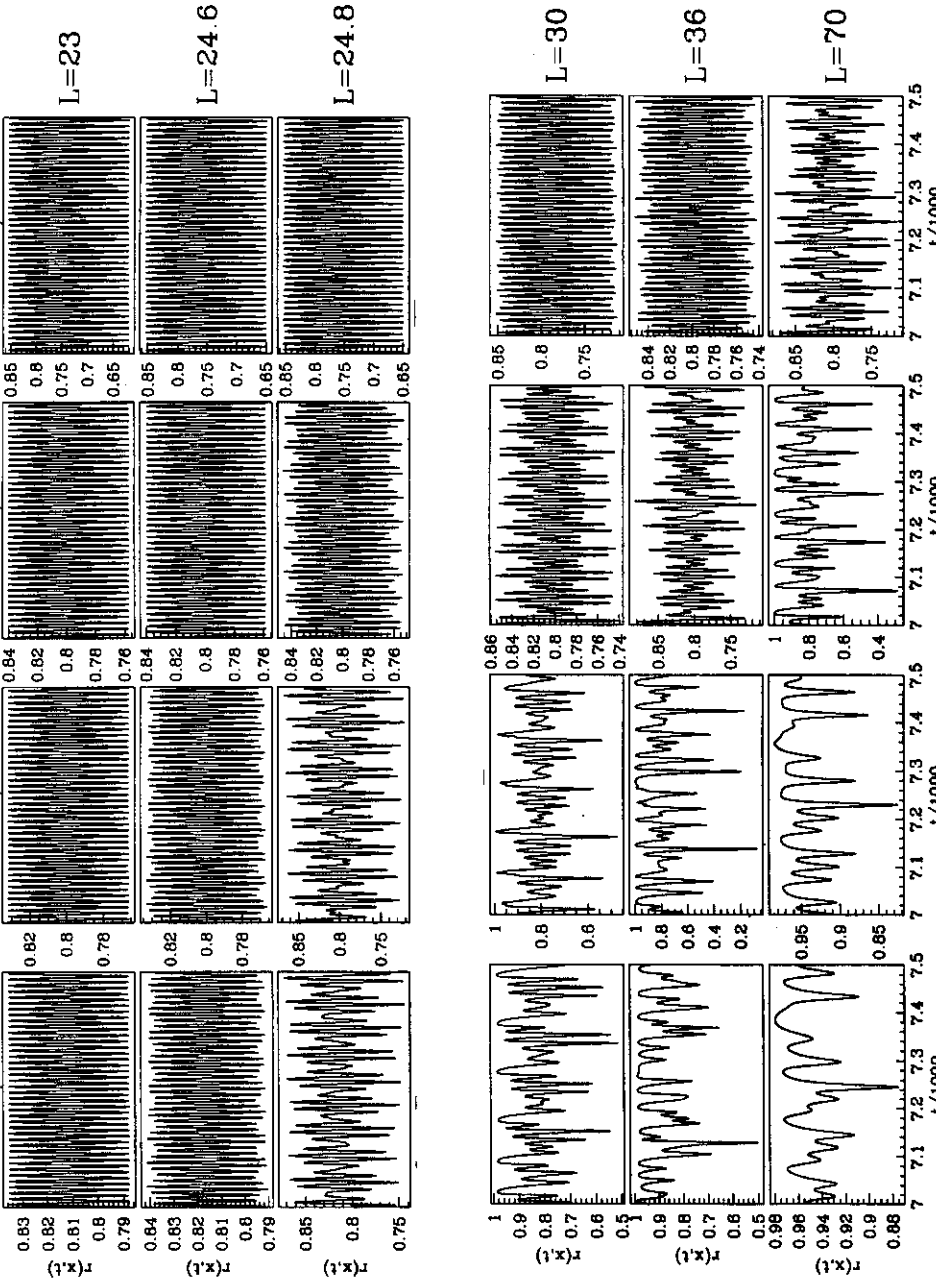
x=L/11
x=3L/11
x=7L/11
x=9L/11
L=23
L=24.6
L=24.8
L=30
L=36
L=70
r(x,t)
t/1000

oscillations. However, in contrast to the case described above, this behaviour does not occur synchronously in x. Rather, the bifurcation occurs initially near $x=0$, and then a 'wave of bifurcation' moves across the domain, as illustrated in Fig. 8. Thus, for some values of L there are irregular oscillations in r near $x=0$, but regular oscillations near $x=L$.

For other values of r^* that I have investigated, the progression to irregular oscillations has one of these two forms, although in some cases I have been unable to detect any intermediate steps between simple periodic oscillations and irregularities. I assume that this is because the transition occurs very rapidly as L is increased, and that I have failed to select an L value in the transition region.

The key implication of these results is that the observation of period-doubling cascades and quasi-periodicity, which are standard routes to chaos in ODE systems, strongly indicate that the irregular temporal oscillations observed in these finite domain computations for large L are genuinely chaotic. This is a new observation for reaction–diffusion equations, although the approach of taking the domain length as a bifurcation parameter in a route to chaos has been used previously for the complex Ginzburg–Landau equation, demonstrating transitions to chaos via two- and three-tori (Keefe, 1985; Moon *et al.*, 1983; Sirovich *et al.*, 1990). Chaos in the complex Ginzburg–Landau equation has of course been very well studied (e.g. Shraiman *et al.*, 1992; Van Saarloos & Hohenberg, 1992). The key difference between this equation and (1) is that the complex Ginzburg–Landau equation is studied in a parameter region in which the spatially homogeneous oscillations (corresponding to the limit cycle of the kinetics) are unstable due to high cross-diffusion; this results in quite different dynamics.

My initial motivation for using domain length L as a bifurcation parameter was that the length of the wake region grows as an imposed function of time, so that one can think of the bifurcation having an imposed variation with time. However, there is an additional complication in the case of oscillatory wakes, namely that the boundary condition (7) does not apply at both ends of the growing domain, but rather only at the moving boundary. In fact, the zero-flux boundary condition at $x=0$ is not significant in the solutions, and if it is replaced by condition (7), there is no significant change in either the moving-boundary or semi-infinite-domain simulations (not illustrated for brevity); rather there is just a localized difference near the $x=0$ boundary. However, there can be significant differences in the behaviour on fixed-length domains, such as that illustrated in Figs 7 and 8, if the boundary condition at $x=0$ is changed to zero flux. If the bifurcations are occurring at relatively large values of L, the sequence of long-term temporal behaviours near the $x=L$ boundary is barely altered by changing to a zero-flux condition at $x=0$; for example, for the parameters used in Fig. 8, there is still a progression to temporal irregularity via quasi-periodicity. However, the sequences for small values of x are changed significantly, and in particular the progression to

Fig. 8. Bifurcations in long-term behaviour of λ–ω solutions on a finite domain. The solutions illustrated are for equations (1) on $0<x<L$ with $\lambda(r)=1-r^2, \omega(r)=3-r^2$ subject to boundary condition (7) at $x=0$ and $x=L$, with $r^*=0.535$. The solution for r is plotted as a function of time t at four different x values. In this case, the irregular oscillations arise through apparent bifurcations to tori in the long-term temporal behaviour; however, in contrast to the case shown in Fig. 7, the transitions do not occur synchronously in x, but rather through a 'wave of bifurcation' moving across the domain in the positive x direction. The equations were solved numerically using the method of lines and Gear's method.

temporal irregularity does not occur through bifurcation sequences that are recognizable from ODE dynamics. Moreover, when bifurcations occur at smaller values of L (e.g. Fig. 7), the sequence of long-term temporal behaviours is altered significantly throughout the domain, and again recognizable bifurcation sequences are often lost. This is unsurprising since the periodic travelling wave itself does not satisfy the zero-flux conditions, so that even for very small values of the domain length L, the long-term solution for r is spatially varying.

Within this proviso, the results described in this section indicate that one can think intuitively of the wake region as being in a perpetual transient on the way to temporal chaos. A useful analogy is an ODE system in which a bifurcation parameter has an imposed variation with time: the long-term behaviour passes through a sequence of bifurcations leading to chaos, but the solution never has the chance to settle down to this long-term behaviour because the parameters are continually changing.

5 Predator–prey dynamics on growing domains

In this section, I move away from λ–ω systems to consider the application of the growing domains idea to more general reaction–diffusion systems. I focus on the example of predator–prey interactions, although the choice of this as opposed to another oscillatory phenomenon is essentially arbitrary. I am really using the predator–prey case simply as an example of a non-λ–ω system, and I will discuss the ecological implications of oscillatory wakes only briefly (in Section 6), since these are described at length elsewhere (Sherratt *et al.*, 1995, 1996). Reaction–diffusion models for predator–prey interaction have the general form

$$\frac{\partial p}{\partial t}=\frac{D_p\partial^2 p}{\partial x^2}+f_p(p, h) \tag{14a}$$

$$\frac{\partial h}{\partial t}=\frac{D_h\partial^2 h}{\partial x^2}+f_h(p, h) \tag{14b}$$

(Murray, 1989). Here $p(x, t)$ and $h(x, t)$ represent predator and prey densities, and are functions of the one-dimensional spatial coordinate x and time t. Realistic kinetic terms f_p and f_h have two non-trivial steady states: a 'prey-only state' in which $p=0$, and a 'coexistence state', in which both p and h are non-zero, say $p=p_s$, $h=h_s$. In many predator–prey models, there are realistic parameter regions in which this coexistence steady state is in fact unstable, with a stable limit cycle in the kinetics, reflecting the oscillatory dynamics of many real predator–prey systems (Nisbet & Gurney, 1982). In such cases, spatially localized perturbation of the coexistence steady state gives rise to either regular or irregular oscillatory wakes, as illustrated in Fig. 1.

As soon as one moves away from λ–ω systems, one is immediately handicapped by the lack of a coordinate system analogous to the r–θ representation (3). Therefore, the moving-boundary condition (7) has no analogue for more general systems, and the only boundary condition that can be used to force a periodic wave is to specify the reaction–diffusion variables as functions of time, in a manner analogous to condition (8). Moreover, again in sharp contrast to λ–ω systems, there is no analytical expression for the periodic waves in the system (14); however, for the purposes of numerical simulation this is not a major difficulty, since the

periodic wave form can be calculated numerically to a high degree of accuracy, using a method which I will now outline.

Periodic travelling waves correspond to a limit cycle solution of the ODE system

$$\frac{D_p \mathrm{d}^2 P}{\mathrm{d}z^2} + \frac{a \mathrm{d}P}{\mathrm{d}z} + f_p(P, H) = 0 \tag{15a}$$

$$\frac{D_h \mathrm{d}^2 H}{\mathrm{d}z^2} + \frac{a \mathrm{d}H}{\mathrm{d}z} + f_h(P, H) = 0 \tag{15b}$$

Here $h(x, t) = H(z; a)$ and $p(x, t) = P(z; a)$ are the travelling wave solutions; $z = x - at$ is the travelling wave coordinate, with a the wave speed. The periodic travelling waves arise from a Hopf bifurcation in these ODEs, which occurs at some critical value, a_{hopf} say, as a is increased with all other parameters fixed (Kopell & Howard, 1973). It is this Hopf bifurcation to periodic waves that enables their form to be calculated numerically. The bifurcating branch of periodic waves, $P_{\text{per}}(z; a)$ and $H_{\text{per}}(z; a)$ say, can be found numerically in a standard way, and then tracked by numerical continuation; I have used the package AUTO for this (Doedel *et al.*, 1991).

The purpose of the moving-boundary simulation for predator–prey systems is to represent in a simpler way the oscillatory wakes such as those illustrated in Fig. 1. In this case, I have been unable to determine a formula for the speed or period of the regular periodic waves immediately behind the invasive front; however, this speed c_{ppw}, and also the front speed c_{bndy}, can be calculated easily from semi-infinite-domain simulations (see the legend to Fig. 9 for details). The combination of a value for this speed together with the numerical form for the periodic waves enables the boundary condition

$$p = P_{\text{per}}(c_{\text{bndy}} t + c_{\text{ppw}} t; c_{\text{ppw}}) \quad \text{and} \quad h = H_{\text{per}}(c_{\text{bndy}} t + c_{\text{ppw}} t; c_{\text{ppw}}) \tag{16}$$

to be imposed at the moving boundary. In Fig. 9, I compare the solution of the moving-boundary problem subject to condition (16) with the oscillatory wake behind invasion, for one particular predator–prey model; details of the equations and boundary conditions are given in the figure legend. The comparison is extremely good, both in this case and for a range of other parameter values. Moreover, as for λ–ω systems, as the boundary speed c_{bndy} is increased with fixed c_{ppw}, the length of the band of regular oscillations increases (not illustrated for brevity).

In the λ–ω case, I was able to link these moving boundary simulations to simple bifurcation sequences on stationary domains. Unfortunately, this is not possible for more general systems such as predator–prey models. There are two basic difficulties. The first is that there is no analogue of the periodic wave amplitude r that can be plotted to study bifurcations. This may seem a minor problem, but in fact the temporal oscillations in amplitude that occur when the periodic wave becomes unstable have a frequency that is quite unrelated to the frequency of the initial periodic waves. This makes it almost impossible to detect bifurcations from plots of numerical solutions of the original partial differential equation (PDE) variables. In fact, I have been able to get around this difficulty by calculating numerically the shortest distance between the current solution point and the projection of the periodic wave limit cycle on to the h–p plane. Even though I only

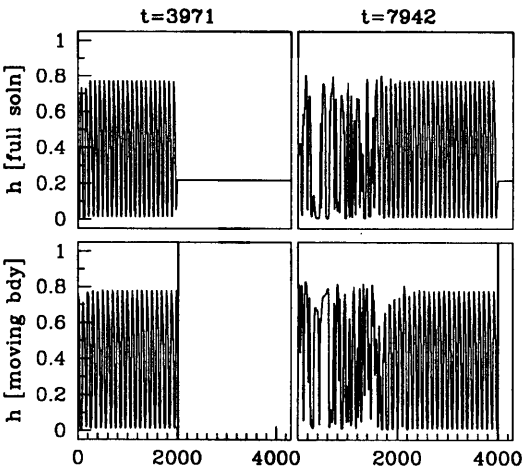

Fig. 9. A comparison between semi-infinite-domain (marked 'full soln') and moving-boundary solutions for the predator–prey system (14) with $f_h(p, h) = h(1-h) - p(1-e^{-Ch})$, $f_p(p, h) = Bp(A-1-Ae^{-Ch})$, which is a standard predator–prey model and has oscillatory kinetics for suitable values of the parameters A, B and C (Murray, 1989). The case illustrated is $A=1.5$, $B=0.05$, $C=5$, $D_p = D_h = 1$. In the semi-infinite-domain solution, the initial conditions are that the system is in the coexistence steady state $h = h_s \equiv (1/C)\log[A/(A-1)]$, $p = p_s \equiv Ah_s(1-h_s)$ everywhere except near the $x=0$ boundary, where a small, localized perturbation is applied. In the moving-boundary simulation, the condition (16) is used on the moving boundary, with the periodic wave forms $P_{\text{per}}(\cdot)$ and $H_{\text{per}}(\cdot)$ calculated as described in the main text. The speed c_{bndy} of the moving boundary is taken to be the speed of the front in the semi-infinite-domain simulations, which can easily be found numerically. However, when $D_h = D_p$, the linearization about the coexistence steady state shows that the front speed has a minimum value of $[2\partial f_h/\partial h + 2\partial f_p/\partial p]^{1/2}|_{(p=p_s, h=h_s)}$, and in numerical simulations it is this minimum front speed that is observed. For the parameters used in the figure, this gives a front speed ≈ 0.313. The speed c_{ppw} of the periodic waves forced on the boundary is determined from the semi-infinite-domain simulation, and here $c_{\text{ppw}} = 1.504$ is used. The simulations are very sensitive to the value of c_{ppw}, particularly the length of the region of regular oscillations. A preliminary estimate of c_{ppw} can be calculated as the ratio of the space and time periods of the regular oscillations in the semi-infinite-domain simulation, but this is not sufficiently accurate. Therefore the practice has been adopted of refining this estimate by plotting the regular oscillations in the h–p plane, and comparing the resulting loop with the projection of the periodic wave limit cycle. Even a visual comparison of these two loops typically enables c_{ppw} to be calculated to three or four significant figures. The prey density $h(x, t)$ only is illustrated, but the predator density $p(x, t)$ has a qualitatively very similar form. The equations were solved numerically using a Crank–Nicolson finite difference scheme, as discussed in the appendix.

have a numerical representation of the limit cycle, this procedure is quite easy to automate.

However, I was unable to circumvent the more serious difficulty of not having suitable boundary conditions to use in a bifurcation study. As I have discussed, there is no analogue of the condition (7) used in the λ–ω case, and the only possibility is the condition (16). However, this imposition of the reaction–diffusion variables as functions of time on the boundaries does not give a recognizable bifurcation sequence, either in the predator–prey or λ–ω cases.

Nevertheless, the moving-boundary results for predator–prey systems do have important implications for the oscillatory wakes phenomenon. In the case of λ–ω systems, there is a strong mathematical basis for the idea that the rear of the leading front effectively imposes a boundary condition on the wake region, namely the structure of the solution as a transition wave in r and θ_x. In more general

reaction–diffusion systems such as the predator–prey model (14), I have previously conjectured that the same mechanism applies (Sherratt, 1994a), and the moving-boundary results strongly suggest that this conjecture is correct. That is, the strong similarity between the moving-boundary solutions and the oscillatory wakes behind invasion provides good evidence that the invasive front really can be regarded as determining the solution in the wake region by forcing a particular periodic wave at its boundary.

6 Discussion

In this paper, I have described the way in which the solution of oscillatory reaction–diffusion equations on growing domains can be used to mimic oscillatory wake phenomena. This has provided strong evidence that the advancing wave front can correctly be thought of as forcing a particular periodic wave at the boundary of the wake region. For λ–ω systems, this had already been established for regular wakes, but the work represents a new result for the case of wholly irregular wakes in λ–ω systems and more generally for other reaction–diffusion systems. In addition, for λ–ω systems, the combination of moving-boundary results and bifurcation studies suggests that irregular wakes have the form of a perpetual transient in a progression towards chaos.

Many real biological systems are oscillatory, and I will now briefly review the application of the oscillatory wakes phenomenon to the specific cases of intracellular calcium signalling and predator–prey invasion. Further details are given elsewhere (Sherratt *et al.*, 1995, 1996; Sneyd & Sherratt, 1996). Calcium is an important intracellular second messenger, and exhibits a wide range of spatial and temporal oscillations in response to different extracellular signals (see Tsien & Tsien, 1990, for a review). The essential biological sequence is that external stimulation causes cells to produce a regulatory molecule known as IP_3. This in turn induces calcium release from intracellular stores, through channels that are IP_3-sensitive. Subsequent calcium release is then auto-regulated by the extracellular calcium level. The dynamics of this process has been extensively modelled (see Sneyd *et al.*, 1995, for a review). Typically, depending on the IP_3 concentration (which can be regarded as a parameter), models are either excitable or oscillatory, and in the oscillatory regime, simulation of calcium signalling waves reveals exactly the oscillatory wake structure. That is, a leading wave front moves across the domain (speed about 2 $\mu m\, s^{-1}$), behind which are periodic waves moving in the opposite direction, and with a much greater speed (about 30 $\mu m\, s^{-1}$).

The invasion of prey populations by a predatory species has been extensively studied, both theoreticaly and in field studies (for example, Kot, 1992; Lehman & Caceres, 1993). However, until very recently, invasion had not been simulated theoretically for predator–prey systems with oscillatory population kinetics; many real predator–prey systems are in this category. With co-workers, I have shown (Sherratt *et al.*, 1995, 1996) that for a range of standard predator–prey models, of both reaction–diffusion and other types, localized introduction of predators into a prey population leads to an invasive wave front, behind which there is an oscillatory wake, with either regular or irregular oscillations, depending on kinetic parameters. This invasive solution is fundamentally different from that illustrated in Fig. 1, which is also a solution of a predator–prey model, because in Fig. 1 the system is in the mixed prey–predator steady state ahead of the leading front, whereas ahead of an invasive wave front, the system is in the prey-only steady state. Nevertheless,

the phenomenon is the same: in invasion, the solution approaches the mixed prey–predator equilibrium transiently, and the oscillatory wake arises as a direct consequence of this transient.

Many chemical systems are also oscillatory, including the famous Belousov–Zhabotinskii reaction, and these systems provide the most feasible situation for detailed experimental observation of oscillatory wakes. In such systems, it is not possible to apply spatially localized perturbations, because the system can never be started exactly at the unstable equilibrium state. However, in this context, the moving boundary approach that I have used in this paper has an additional application, quite different from the mathematical aspects on which I have focused. Namely, moving boundaries provide a feasible method of observing oscillatory wakes in chemical systems, because it is possible to reproduce oscillating boundary conditions experimentally. This was done recently by Stössel and Münster (1995), for the Belousov–Zhabotinskii reaction in a silica gel. The details of their experimental scheme mean that the system is in fact excitable rather than oscillatory in the reaction vessel, but otherwise their method is directly applicable to the observation of oscillatory wakes. Specifically, they use an effectively one-dimensional reaction vessel at the ends of which temporal oscillations are imposed in the concentraiton of reactants. If this method were amended so that the system were oscillatory in the reaction vessel and one of the boundaries was moveable, then the work I have presented predicts that oscillatory wakes will be observed. Specifically, I predict a transition from spatio-temporal irregularities to periodic travelling waves in the unstirred part of the reaction vessel, as the speed of the moving partition is increased.

Acknowledgements

This work was supported in part by grants from the Nuffield Foundation and the Royal Society of London. I am grateful to Andrew Fowler (University of Oxford, UK), Mark Lewis (University of Utah, USA), Barry Eagan (University of Utah, USA) and James Sneyd (University of Canterbury, New Zealand) for helpful discussions.

References

Atri, A., Amundson, J., Clapham, D. and Sneyd, J. (1993) A single pool model for intracellular calcium oscillations and waves in the *Xenopus laevis* oocyte. *Biophysics Journal* **65**, 1727–1739.

Breitenmoser, U., Slough, B. G. and Breitenmoserwursten, C. (1993) Predators of cyclic prey—is the Canada lynx victim or profiteer of the snowshoe hare cycle. *Oikos* **66**, 551–554.

Chakravarti, S., Marek, M. and Ray, W. H. (1995) Reaction–diffusion system with Brusselator kinetics—control of a quasi-periodic route to chaos. *Physical Review E* **52**, 2407–2423.

Dew, P. M. and Walsh, J. E. (1980) A set of library routines for the numerical solution of parabolic equations in one space variable. *University of Manchester Numerical Analysis Report* **49**.

Doedel, E., Keller, H. B. and Kernevez, J. P. (1991) Numerical analysis and control of bifurcation problems I: bifurcations in finite dimensions. *International Journal of Bifurcation and Chaos* **1**, 493–520.

Ermentrout, G. B. (1980) Small amplitude stable wavetrains in reaction–diffusion systems. *Lecture Notes in Pure and Applied Mathematics* **54**, 217–228.

Field, R. J. and Burger, M. (eds) (1985) *Oscillations and Travelling Waves in Chemical Systems* (Wiley, New York).

Howard, L. N. and Kopell, N. (1977) Slowly varying waves and shock structures in reaction–diffusion equations. *Studies in Applied Mathematics* **56**, 95–145.

Keefe, L. R. (1985) Dynamics of perturbed wave train solutions to the Ginzburg–Landau equation. *Studies in Applied Mathematics* **73**, 91–153.

Koga, S. (1982) Rotating spiral waves in reaction–diffusion systems. Phase singularities of multi-armed waves. *Progress in Theoretical Physics* **67**, 164–178.

Kopell, N. and Howard, L. N. (1973) Plane wave solutions to reaction–diffusion equations. *Studies in Applied Mathematics* **52**, 291–328.

Kot, M. (1992) Discrete time travelling waves: ecological examples. *Journal of Mathematical Biology* **30**, 413–436.

Lehman, J. T. and Caceres, C. E. (1993) Food-web responses to species invasion by a predatory invertebrate—*Bythotrehes* in Lake Michigan. *Limnology and Oceanography* **38**, 879–891.

Moon, H. T., Huerre, P. and Redekopp, L. G. (1983) Transitions to chaos in the Ginzburg–Landau equation. *Physica D* **7**, 135–150.

Murray, J. D. (1989) *Mathematical Biology* (Springer, Berlin).

Nisbet, R. M. and Gurney, W. S. C. (1982) *Modelling Fluctuating Populations* (Wiley, New York).

Norbury, J. and Stuart, A. M. (1988) Travelling combustion waves in a porous medium. Part I—existence. *SIAM Journal of Applied Mathematics* **48**, 155–169.

Norbury, J. and Stuart, A. (1989) A model for porous medium combustion. *Quarterly Journal of Mechanics and Applied Mathematics* **42**, 159–178.

Paullet, J., Ermentrout, B. and Troy, W. (1994) The existence of spiral waves in an oscillatory reaction–diffusion system. *SIAM Journal of Applied Mathematics* **54**, 1386–1401.

Sanderson, M. J., Charles, A. C. and Dirksen, E. R. (1990) Mechanical stimulation and intercellular communication increases intracellular Ca^{2+} in epithelial cells. *Cell Regulation* **1**, 585–596.

Sherratt, J. A. (1993) The amplitude of periodic plane waves depends on initial conditions in a variety of λ–ω systems. *Nonlinearity* **6**, 1055–1066.

Sherratt, J. A. (1994a) Irregular wakes in reaction–diffusion waves. *Physica D* **70**, 370–382.

Sherratt, J. A. (1994b) On the evolution of periodic plane waves in reaction–diffusion equations of λ–ω type. *SIAM Journal of Applied Mathematics* **54**, 1374–1385.

Sherratt, J. A. (1995) Unstable wavetrains and chaotic wakes in reaction–diffusion systems of λ–ω type. *Physica D* **82**, 165–179.

Sherratt, J. A., Lewis, M. A. and Fowler, A. C. (1995) Ecological chaos in the wake of invasion. *Proceedings of the National Academy of Sciences of the USA* **92**, 2524–2528.

Sherratt, J. A., Eagan, B. T. and Lewis, M. A. (1996) Oscillations and chaos behind predator–prey invasion: mathematical artifact or ecological reality? *Philosophical Transactions of the Royal Society B* (in press).

Shraiman, B. I., Pumir, A., Van Saarloos, W., Hohenberg, P. C., Chate, H. and Holen, M. (1992) Spatiotemporal chaos in the one dimensional complex Ginzburg–Landau equation. *Physica D* **57**, 241–248.

Sirovich, L., Rodriguez, J. D. and Knight, B. (1990) Two boundary value problems for the Ginzburg–Landau equation. *Physica D* **43**, 63–76.

Sneyd, J. and Sherratt, J. A. (1996) On the propagation of calcium waves in an inhomogeneous medium. *SIAM Journal of Applied Mathematics* (in press).

Sneyd, J., Keizer, J. and Sanderson, M. J. (1995) Mechanisms of calcium oscillations and waves: a quantitative analysis. *FASEB Journal* **14**, 1463–1472.

Stössel, R. and Münster, A. F. (1995) Periodic and irregular wave patterns in an open tubular gel reactor. *Chemical and Physical Letters* **239**, 354–360.

Tsien, R. W. and Tsien, R. Y. (1990) Calcium channels, stores and oscillations. *Annual Review of Cell Biology* **6**, 715–760.

Van Saarloos, W. and Hohenberg, P. C. (1992) Fronts, pulses, sources and sinks in generalized complex Ginzburg–Landau equations. *Physica D* **56**, 303–367.

Appendix: Numerical methods

There are two basic approaches to numerical solution of the moving-boundary problems discussed in this paper, namely either to incorporate the moving boundary directly into the numerical scheme, or to change variables to give a fixed domain, and solve in these transformed coordinates. I have used both approaches to verify my numerical results, and I now describe the methods in more detail.

Explicit inclusion of the moving boundary in the numerical scheme can be done

most conveniently with a simple finite difference numerical method, and I have used a semi-implicit Crank–Nicolson scheme, in which the diffusion terms are represented by central differences, with their values at the current and previous time steps averaged. For a system of the form (14), this gives

$$\frac{p_i^{j+1}-p_i^j}{\delta t}=\frac{D_p}{2}\frac{p_{i+1}^{j+1}-2p_i^{j+1}+p_{i+1}^{j+1}}{\delta x^2}+\frac{D_p}{2}\frac{p_{i+1}^{j}-2p_i^{j}+p_{i-1}^{j}}{\delta x^2}+f_p(p_i^j, h_i^j)$$

and similarly for (14b). Here p_i^j denotes the variable at space-point i and time-iteration j, and δt and δx are the time and space steps, which I take to be constant. This gives a tridiagonal system of linear algebraic equations to be solved at each time iteration. I have found that this is more efficent than a fully implicit scheme in which the kinetics are also evaluated at the new time step, because even though larger time steps can then be used for a given accuracy, this does not compensate for the extra time required to solve nonlinear algebraic equations at each iteration. Within the context of this finite difference scheme, I include the moving boundary in a very simple way, by restricting solution to the mesh points $1\leq i\leq i_{\max}=\mathrm{int}(c_{\mathrm{bndy}}j\delta t/\delta x)$, with the moving-boundary condition applied at mesh point $i=i_{\max}$.

A quite different numerical approach is to start by changing variables to give a stationary domain. The appropriate transformation is $X=x/(c_{\mathrm{bndy}}t)$, $T=t$, under which a system such as (14) becomes

$$\frac{\partial p}{\partial T}=\frac{D_p}{c_{\mathrm{bndy}}^2T^2}\frac{\partial^2 p}{\partial X^2}+\frac{X}{T}\frac{\partial p}{\partial X}+f_p(p, h)$$

and similarly for (14b). The appropriate solution domain is then $0<X<1$, and boundary conditions involving spatial derivatives must be transformed appropriately. This transformed system could be solved by a number of numerical methods, including the finite difference scheme described above, but to maximize the difference between my two methods I have instead used the method of lines and Gear's method, which is implemented in the NAG library. The method of lines simply converts the PDEs to a system of coupled ODEs using a simple spatial discretization, which I take to be uniform; Gear's method is a variable-order, variable-step ODE solver, based on backwards differentiation formulae (for details, see Dew & Walsh, 1980). Of course, solution of these transformed equations must be started at a small finite value of T, rather than at $T=0$, but details of the initial solution used appear to have only a transient influence on the solution.

These two numerical methods have no relationship but give the same results, which is strong evidence that the numerical solutions are good approximations to the true solutions. The finite difference and Gear methods can also both be used to solve the semi-infinite-domain problem, which is rather more straightforward numerically, and again the methods agree.